J. Meas. Sci. Instrum., 2024, 15(4): 558-570.
DOI: 10.62756/jmsi.1674-8042.2024055
http://jmsi.publish.founderss.cn
jmsi@nuc.edu.cn

Fault diagnosis method of AC motor rolling bearing based on heterogeneous data fusion of current and infrared image

LIU Peijin[1], GUO Zichen[1], HE Lin[2*], YAN Dongyang[1], ZHANG Xiangrui[1]

1. College of Mechatronics Engineering, Xi'an University of Architecture and Technology, Xi'an 710055, China;
2. College of Science, Xi'an University of Architecture and Technology, Xi'an 710055, China

***Corresponding author:** HE Lin (helin716@163.com)

Received: November 12, 2023 **Revised:** December 28, 2023 **Accepted:** January 17, 2024

Abstract: In order to improve the accuracy of rolling bearing fault diagnosis when the motor is running under non-stationary conditions, an AC motor rolling bearing fault diagnosis method was proposed based on heterogeneous data fusion of current and infrared images. Firstly, VMD was used to decompose the motor current signal and extract the low-frequency component of the bearing fault signal. On this basis, the current signal was transformed into a two-dimensional graph suitable for convolutional neural network, and the data set was classified by convolutional neural network and softmax classifier. Secondly, the infrared image was segmented and the fault features were extracted, so as to calculate the similarity with the infrared image of the fault bearing in the library, and further the sigmod classifier was used to classify the data. Finally, a decision-level fusion method was introduced to fuse the current signal with the infrared image signal diagnosis result according to the weight, and the motor bearing fault diagnosis result was obtained. Through experimental verification, the proposed fault diagnosis method could be used for the fault diagnosis of motor bearing outer ring under the condition of load variation, and the accuracy of fault diagnosis can reach 98.85%.
Key words: current signal; infrared image; decision level fusion; rolling bearing; fault diagnosis

0 Introduction

Rolling bearings are an important part of most rotating machinery, and rolling bearing failure is the main cause of functional failure of equipment[1-3]. According to relevant statistics, about 40% of motor failures are caused by bearing failures[4]. Therefore, the timely and accurate identification of faults in rolling bearings when they occur is of great importance to motor operation and maintenance and safe production.

In rolling bearing fault diagnosis research, the use of vibration signals for research is more mature and widely used[5], but the vibration signal acquisition will be affected by the arrangement of measurement points, which will interfere with the acquired vibration signals and affect the accuracy of motor bearing fault diagnosis. Motor current signature analysis (MCSA), as a non-invasive bearing fault diagnosis method, still has good results in fault diagnosis research, although its application to bearing fault diagnosis is late. The radial and torsional motion transfer models of bearing are established, and the relationship between the characteristic components of bearing vibration and current sideband fault harmonics is revealed[6,7]. Song et al.[8] found a characteristic component of a bearing failure that would be revealed because the bearing failure was influenced by the inherent eccentricity of the motor and the cogging effect. Chu et al.[9] obtained the analytical signal model of the stator current in case of motor bearing failure by solving the equivalent magnetic circuit method. Karatzinis et al.[10] proposed an approach using a fuzzy cognitive network (FCN) with functional weights. So far the majority of studies using MCSA for fault diagnosis of motor rolling bearing outer ring are under constant speed and constant load conditions, while there is a lack of sufficient scientific research for non-smooth operating conditions.

Infrared images can be used to characterize the operating state of the object under test by its temperature field distribution. The abnormal monitoring of blower bearings and motor operating conditions in nuclear power plant ventilation systems was successfully performed with the help of thermal imaging[11]. Sun et al.[12] established a motor bearing fault for simulation by finite element and conducted experiments, and proposed that the motor end surface temperature distribution could be used as a basis for motor bearing fault judgment. Azeez et al.[13] measured the

temperature during bearing failure by thermal imaging and found that thermal imaging could be used to distinguish between different types of rolling element failures. However, infrared images can be affected by multiple parameters such as ambient temperature, operating time, and bearing load, thus producing errors in bearing fault diagnosis results.

There are information redundancy and differences in different signals, and the reliability of the fused signals can be improved by analyzing the redundancy among the compared signals, and the information content of the fused signals can be increased by analyzing the characteristics of the compared signals. The raw data from multiple motor sensors was used as input and the different data was fused through deep learning, so that the motor fault diagnosis method gradually was improved[14]. Hou et al.[15] fused the vibration signal as well as the stator current signal for analysis to improve the reliability of rolling bearing fault diagnosis in induction motors. In the current research on rolling bearing fault diagnosis, there are few reports on the fusion of two types of heterogeneous data for rolling bearing fault diagnosis by making full use of motor operating current and infrared image signals. Wang et al.[16] used fusion of power timing parameters as well as power image parameters for sensing transmission line ice coverage levels and distribution cable discharge defects to improve the accuracy of sensing.

Heterogeneous data fusion was used to make full use of the information redundancy and complementary characteristics of motor current signal and bearing infrared image to improve the accuracy of bearing fault diagnosis in this paper. A heterogeneous data fusion model applicable to motor stator current signal and infrared image signal was established. The main idea was to preprocess the motor current signal by variational modal decomposition to extract the signal in the low frequency band where the bearing fault signal was located, based on which the current signal was transformed into a two-dimensional map applicable to neural networks, and the data set was classified by using convolutional neural networks (CNN) and softmax classifier. At the same time, the infrared image was segmented, fault features were extracted, and the similarity with the infrared image of the faulty bearing in the library was calculated. Then the sigmod classifier was used to classify the data. Finally, a decision-level fusion method was introduced to fuse the diagnostic results of current signal and infrared image signal by weight to obtain the motor bearing fault diagnosis results. The model as a motor rolling bearing fault diagnosis can simplify the motor rolling bearing fault diagnosis operation, and effectively improve the accuracy and fault tolerance of bearing fault diagnosis.

1 Heterogeneous data fusion fault diagnosis method

Multi-source data fusion methods are classified into data level, feature level, and decision level according to the different fusion levels. The level of data fused by data-level fusion and feature-level fusion is low, which has strict requirements for sensor alignment and spatiotemporal coherence of multi-source data. The difference of different signal sources will also affect the fusion result. Decision-level fusion methods are higher-level data fusion, and this type of method has good real-time performance and is less affected by data errors. The decision-level fusion method has better fault tolerance as the whole system can get correct results even when the quality of one type of data is poor. The framework of motor information fusion fault diagnosis method is shown in Fig.1.

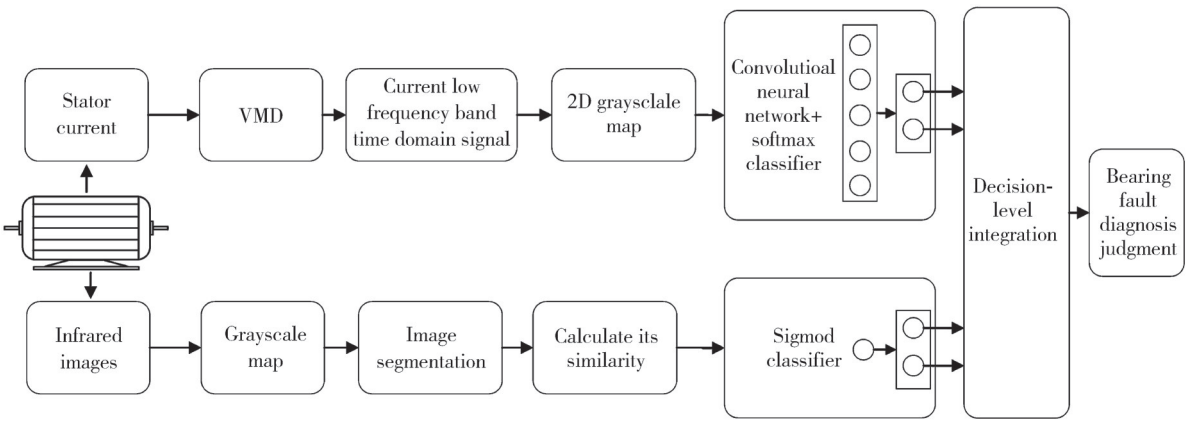

Fig. 1 Overall framework of AC motor rolling bearing fault diagnosis based on current and infrared image data fusion

Firstly, the acquired motor current signal is decomposed by variational modal decomposition (VMD) to obtain the current signal in the low frequency band, on the basis of which the decomposed current signal is transformed into a

two-dimensional gray map suitable for neural networks and classified by a softmax classifier to obtain the classification results. The infrared images taken at the same time are first converted into grayscale maps, and image segmentation is performed to extract the grayscale feature matrix, after which the similarity is calculated with the grayscale feature matrix of the faulty infrared images in the library, and finally the classification is performed by a sigmoid classifier. Finally, the classification results of current and infrared images are fused at decision level and a fault diagnosis verdict is made on the status of the bearing.

2 Current signal and IR image data feature extraction

2.1 Current data feature extraction

2.1.1 VMD-based pre-processing of current signals

Since the motor rolling bearing failure increases the vibration in the full frequency band of the motor, which in turn causes an increase in energy in certain bands in the lower frequency band of the stator current spectrum[17], the acquired current is subjected to VMD to obtain the current signal in the lower frequency band and reduce the irrelevant and redundant information in the current signal. The VMD is an iterative decomposition of the original current signal into intrinsic mode function (IMF). The VMD variational model is[18]

$$\min_{\{u_k\},\{\omega_k\}}\left\{\sum_{k=1}^{K}\left\|\partial_t\left[\left(\delta(t)+\frac{\mathrm{j}}{\pi t}\right)u(t)\right]\mathrm{e}^{-\mathrm{j}\omega_k t}\right\|_2^2\right\},$$

$$\text{s.t.}\sum_{k}^{K}u_k=f, \tag{1}$$

where K is the preset number of decomposed IMFs; $\{u_k\}$ is the kth IMF after decomposition; $\{\omega_k\}$ is the center frequency of the kth IMF; and f is the original current signal.

The problem introduces a quadratic penalty factor α and a Lagrange multiplier λ to transform the constrained variational problem into an unconstrained variational problem. The improved Lagrangian equation is expressed as[19]

$$L\left(\{u_k\},\{\omega_k\},\{\lambda(t)\}\right)=$$
$$\alpha\sum_{k=1}^{K}\left\|\partial_t\left[\left(\delta(t)+\frac{\mathrm{j}}{\pi t}\right)u_t(t)\right]\mathrm{e}^{-\mathrm{j}\omega_k t}\right\|_2^2+$$
$$\left\|f(t)-\sum_{k=1}^{K}u_k(t)\right\|_2^2+\left[\lambda(t),f(t)-\sum_{k=1}^{K}u_k(t)\right]. \tag{2}$$

According to the Ref. [19], iteration can be used in order to solve the variational problem of Eq. (2) and obtain the optimal solution of Eq. (1).

2.1.2 2D grayscale maps generation

In order to facilitate neural network processing, the one-dimensional current signal needs to be converted into a two-dimensional image signal, using a sliding window to split the collected current signal into N samples of equal length, each with n^2 current data, so as to generate a two-dimensional grayscale image for the training of the network, as shown in Fig.2.

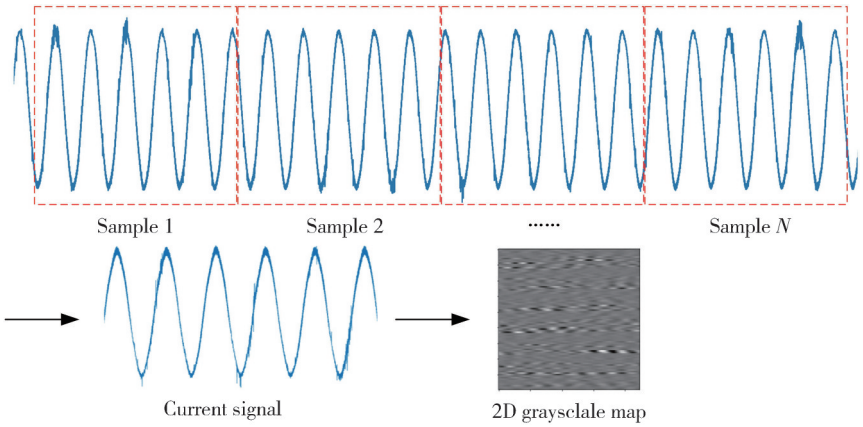

Fig. 2 Two-dimensional diagram of current signal generation

The samples of N current signals are all decomposed by VMD to obtain the low frequency band current signals, and then the decomposed low frequency band current signals are transformed into a matrix of $n\times n$. The transformation method is that the current data of length n^2, one row for each n current data, is arranged row by row in the matrix of $n\times n$. The process can be shown as

$$\begin{bmatrix}a_1 & \cdots & a_{n^2}\end{bmatrix}\rightarrow\begin{bmatrix}a_1 & a_2 & \cdots & a_n\\ a_{n+1} & a_{n+2} & \cdots & a_{2n}\\ \vdots & \vdots & \vdots & \vdots\\ a_{(n-1)n+1} & a_{(n-1)n+2} & \cdots & a_{n^2}\end{bmatrix}. \tag{3}$$

Before transforming the matrix of $n\times n$ into a

grayscale map, it is first necessary to perform a normalization process, as shown in Eq. (4), so that each data value of the matrix of $n \times n$ is in the range of 0—255, to achieve the transformation of one-dimensional current data to two-dimensional grayscale images.

$$a_i' = \frac{a_i - \min a_i}{\max a_i - \min a_i} \times 255, \tag{4}$$

where a_i is the ith current data in the matrix; a_i' is the normalized form; $\max a_i$ and $\min a_i$ are the maximum and minimum values of the current data of the sample matrix, respectively.

2.1.3 Feature extraction networks

According to the actual demand, the two-dimensional image generated for the current signal is diagnosed with or without fault identification. With the increase of the number of layers, the accuracy of the model for motor bearing fault diagnosis is gradually increasing, but too many layers will lead to slow convergence of the model training, so a convolutional neural network with three convolutional layers and three corresponding pooling layers is designed.

To ensure that each pooling layer extracts more local features from the previous pooling layer, in convolution layers 1—3, the convolution kernel sizes are 5×5, 5×5, 3×3, and the numbers are 32, 64, and 128, respectively, with a convolution step of 1 (s=1) and an image boundary filling pattern of SAME. In order to avoid the loss of image features, the pooling layer is chosen as average pooling with a kernel size of 2×2 and a step size of 2 (s=2). Finally, a fully connected layer is used to map the features into a set of one-dimensional data, which are classified by a classifier.

Since the softmax classifier has the advantages of less oversaturation and faster convergence than the sigmod classifier, the softmax classifier is used for classifier selection, and the two outputs correspond to whether the bearing is faulty or not. The final configuration of the convolutional neural network constructed to extract the features is shown in Fig.3.

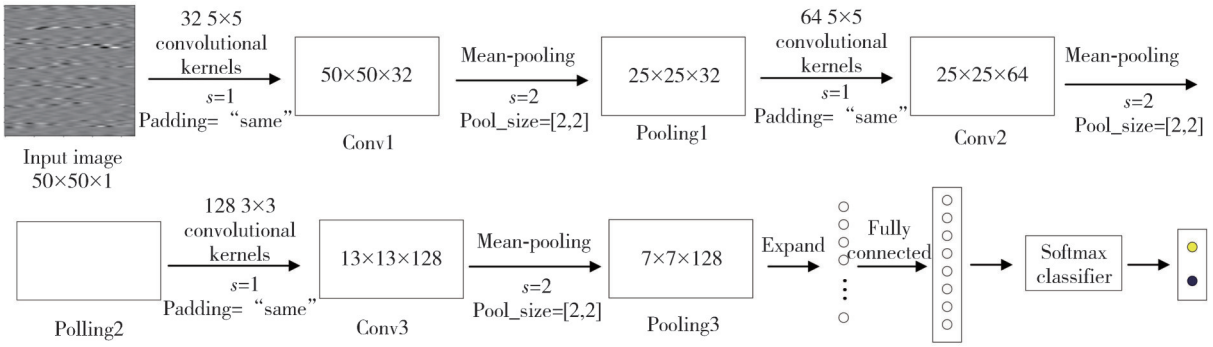

Fig. 3 Two-dimensional image feature extraction network for current signal

The problem of discriminating faults for the softmax classifier is the probability obtained by calculating the value of the input classifier in terms of softmax, i.e.,

$$\boldsymbol{p}(x) = \begin{bmatrix} p(y=1|\boldsymbol{x}) \\ p(y=2|\boldsymbol{x}) \\ \vdots \\ p(y=m|\boldsymbol{x}) \end{bmatrix} = \frac{1}{\sum_{i=1}^{m} \exp x_i} \begin{bmatrix} \exp x_1 \\ \exp x_2 \\ \vdots \\ \exp x_m \end{bmatrix}, \tag{5}$$

where $\boldsymbol{x} = [x_1 \quad x_2 \quad \cdots \quad x_m]^{\mathrm{T}}$ is the input layer of softmax, $\boldsymbol{p}(x)$ is the conditional probability at input $\boldsymbol{x}$; and m is the number of categories to be classified. The probability of each target category with respect to the total target category is calculated by the softmax function, and the target category for a given input is determined based on the calculated probability.

$$H(p', p) = -\sum_{j=1}^{N} p_i' \ln p_i, \tag{6}$$

where $H(p', p)$ is the loss function; p_i is the prediction result; p_i' is the sample really label; and N is the number of samples.

2.2 IR image feature extraction

2.2.1 Image preprocessing and feature extraction

Infrared image acquisition should be carried out at the end of the motor, and the fault feature extraction of infrared image needs to convert the infrared image to gray level image first by

$$Gray = 0.3R + 0.5G + 0.11B. \tag{7}$$

After the grayscale processing of the image, the infrared image is transformed into a grayscale image with grayscale values between 0—255. In order to extract the feature matrix of the infrared image fault features, the infrared fault feature region needs to be defined and divided. The experiments use the basic global thresholding method to binarize the infrared image feature regions, select segmentation thresholds to

capture the target profile information (Fig. 4(a) — 4(c) for normal bearings; Fig. 4(d) — 4(f) for faulty bearings), obtain the grayscale values of the target pixels, and obtain the grayscale feature matrix. Since the grayscale value of the image changes in the range of 0—255 after turning gray, the grayscale values of pixels larger than the selected thresholds are extracted, and the cosine similarity is calculated with the corresponding pixel grayscale values of the faulty infrared images in the fault library.

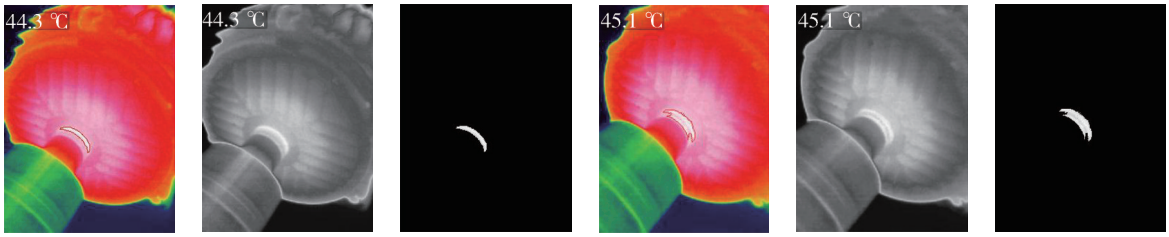

Fig. 4 Motor end cap infrared image binarized image. (a) Normal bearing infrared image; (b) Normal bearing grayscale image; (c) Normal bearing bivariate chart; (d) Faulty bearing infrared image; (e) Faulty bearing grayscale image; (f) Faulty bearing bivariate chart

2.2.2 Calculation of cosine similarity

Cosine similarity uses the cosine of the angle between two vectors in vector space as a measure of the magnitude of the difference between two individuals. The closer the cosine value is to 1, the closer the angle between the two vectors is to 0°, the more similar the two vectors are, and the cosine similarity is calculated by

$$\cos\theta=\frac{\sum_{i=1}^{n}A_iB_i}{\sqrt{\sum_{i=1}^{n}A_i^{\ 2}}\sqrt{\sum_{i=1}^{n}B_i^{\ 2}}}. \tag{8}$$

In this paper, the pixel gray values of the image are used as each element of term A in Eq. (8), and the corresponding pixel gray values in the fault library are used as each element of term B for similarity calculation to be further classified.

2.2.3 Sigmoid classification

Sigmoid is mostly used to do binary classification, which can transform a scalar number to between [0, 1], and if it is greater than the activation threshold, it is considered to belong to a certain category, otherwise it does not belong to that category. In this paper, when classifying infrared images, the sigmoid threshold is adjusted according to the cosine similarity calculated by Eq. (8), and the subsequent infrared image similarity is classified according to the adjusted completed activation function. The sigmoid activation function is

$$y_i=\sigma(\omega x_i+\theta), \tag{9}$$

where $\sigma(t_i=\omega x_i+\theta)=1/(1+\mathrm{e}^{-t_i})$ and θ are the activation thresholds.

$$L(y',y)=-[y'\ln y+(1-y')\ln(1-y)], \tag{10}$$

where $L(y',y)$ is the loss function; y is the predicted outcome; and y' is the true label.

3 Fusion method

3.1 Complementarity analysis

The t-distribution stochastic neighborhood embedding (t-SNE) is a visual analysis method for dimensionality reduction of high-dimensional data. The basic idea is to construct a t-distribution in a low-dimensional space so that it coincides with the probability distribution in a high-dimensional space. The raw data, the current classification output, and the IR image output are used to visualize the layer output of the model using t-SNE, as shown in Fig. 5. As seen in Fig. 5(a) the original current data points are mixed together and indistinguishable. While the majority of the current data can be distinguished in Fig. 5(b), there is a small portion that cannot be distinguished. As shown in Fig. 5(c), the infrared image diagnosis model can distinguish most faults, but there are still many factors, such as operating time, that makes it impossible to accurately determine faults.

The current sample data corresponding to the sample data with wrong diagnosis of infrared image is diagnosed and classified by the current diagnosis model, as shown in Fig. 5(d), which can accurately classify the data with wrong diagnosis. Then the infrared image sample data corresponding to the sample data with wrong diagnosis of current signal is diagnosed and classified by the infrared image diagnosis model, as shown in Fig. 5(e), whose fault diagnosis rate can reach 98.8%. Therefore, the complementary nature of current data and infrared image data can be fully utilized to improve the accuracy of fault diagnosis when performing motor bearing fault diagnosis.

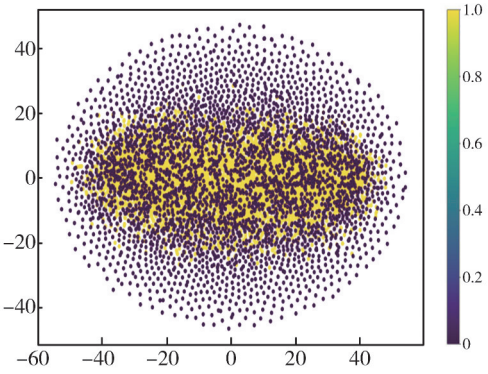

(a) CNN input scatter plot

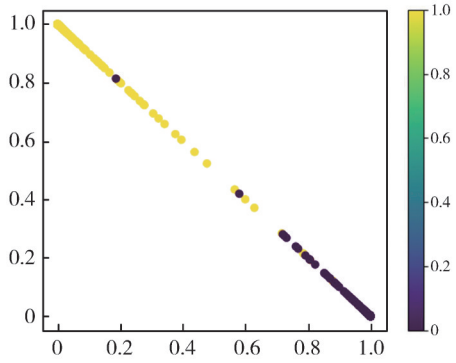

(b) Current classification output scatter plot

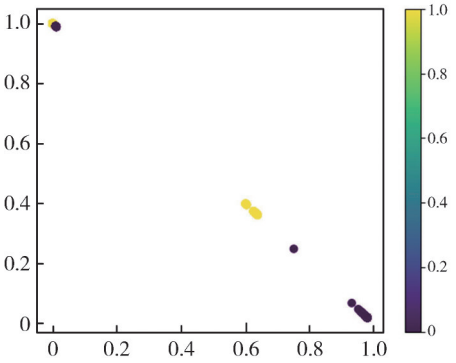

(c) IR classification model output scatter plot

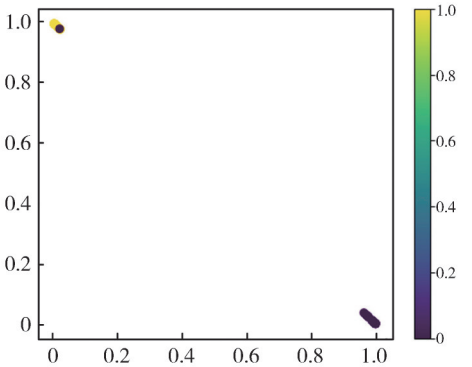

(d) Current supplementary diagnostic output scatter plot

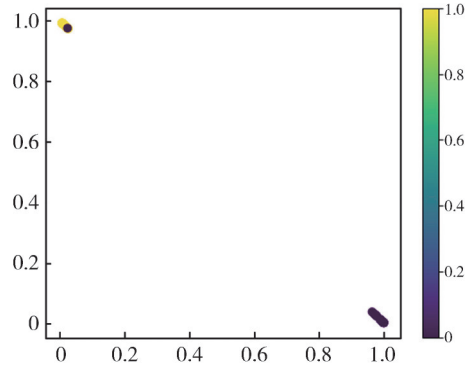

(e) Infrared supplemental diagnostic model output scatter plot

Fig. 5 Complementarity analysis comparison chart

3.2 Decision-level fusion methods

The softmax classifier for current and the sigmoid classifier for infrared images are mentioned, and the results obtained are the probability of whether or not the fault is present, so the decision-level data fusion method is proposed for the classification results of the current signal as well as the infrared image signal. This fusion method is a decision-level fusion method that combines a weighted voting method with a soft voting method for final data fusion. The voting method is widely used in classification problems, where it integrates multiple base classifiers through linear combinations, enabling the integration of complementary information between base classifiers and reducing the classification errors of individual classifiers[19]. The weighted voting method is introduced to effectively reduce the probability of misclassification of the overall data due to misclassification of individual classifiers in the soft voting classification process.

The specific details of this decision-level fusion algorithm are as follows, assuming that there are n data sources $\left[X_1, X_2, \cdots, X_n\right]^{\mathrm{T}}$. The signals from each data source need to be classified into m classes $\left[Y_1, Y_2, \cdots, Y_m\right]^{\mathrm{T}}$. The probability composition of each classification for each data source is

$$
\begin{aligned}
&1)\, X_1 = \left[p_1^1, p_1^2, \cdots, p_1^m\right],\\
&2)\, X_2 = \left[p_2^1, p_2^2, \cdots, p_2^m\right],\\
&\vdots\\
&n)\, X_n = \left[p_n^1, p_n^2, \cdots, p_n^m\right],
\end{aligned}
$$

where p_i^j denotes the probability that X_i data sources are categorically judged to be in category Y_j, where $i=1:n$ and $j=1:m$.

The data $\left[X_1, X_2, \cdots, X_n\right]^{\mathrm{T}}$ are all assigned their corresponding weight factors $\left[W_1, W_2, \cdots, W_n\right]^{\mathrm{T}}$, so the

final probability of type Y_j in m classifications after fusion of the data is

$$1)\ Y_1^p = W_1 p_1^1 + W_2 p_2^1 + \cdots + W_n p_n^1,$$
$$2)\ Y_2^p = W_1 p_1^2 + W_2 p_2^2 + \cdots + W_n p_n^2,$$
$$\vdots$$
$$m)\ Y_m^p = W_1 p_1^m + W_2 p_2^m + \cdots + W_n p_n^m,$$

where Y_j^p indicates the probability of being judged as type Y_j after fusion. The final result is compared, and the type with the highest probability of being obtained is judged to be the type of that data.

There are two sources of data: current data and infrared image data, so $n=2$. And the data is divided into faulty and non-faulty, so $m=2$. Current data are classified into two classes Y_1 and Y_2 with probabilities p_1^1 and p_1^2 by the softmax classifier, and infrared images were also classified into two classes Y_1 and Y_2 with probabilities p_2^1 and p_2^2 by the sigmoid classifier. The weight given to the current data to determine whether the bearing is faulty is W_1, and the weight given to the infrared image to determine whether the bearing is faulty is W_2. After the fusion of current data and infrared image by the fusion method, the probability of judging as Y_1 is $Y_1^p = W_1 p_1^1 + W_2 p_2^1$, and the probability of judging as Y_2 is $Y_2^p = W_1 p_1^2 + W_2 p_2^2$. The Y_1^p and Y_2^p final results are compared and the classification will be judged to correspond to the type with high probability.

3.3 Training of models

The motor heterogeneous data fusion model proposed in this paper is trained as follows.

1) The two-dimensional image generated from the current signal is used as input and the fault classification is used as output to train a fault diagnosis network based on the current two-dimensional image. With the objective of minimizing the cross-entropy loss, iterative training is performed with the Adam gradient descent optimization algorithm with learning rate of 0.01 and smoothing constants $\beta_1=0.9$ and $\beta_2=0.999$.

$$L = \frac{1}{N}\sum_{i=1}^{N} -\left[y_i \ln p_i + (1-y_i)\ln(1-p_i)\right], \quad (11)$$

where y_i denotes the label of sample i, 1 for positive class, and 0 for negative class; p_i denotes the probability that sample i is predicted to be a positive class.

2) The sigmod classifier is trained with the similarity value between the infrared image and the faulty image as the input and the faulty classification as the output, and the loss function of the training objective and the optimization method are the same as 1).

3) The weight factors W_1 and W_2 in the decision-level fusion method are used as training parameters with the objective of minimizing the cross-entropy loss, and the optimization method is the same as 1).

4 Experiments

4.1 Experimental setup and data preparation

4.1.1 Experimental setup

The experimental device consists of three parts: power supply system, motor dragging system, and data acquisition system. The power supply system is 50 Hz industrial frequency power supply. The motor drive system is composed of experimental motor and CZ-10 magnetic powder brake. The experimental motor drives CZ-10 magnetic powder brake to change the motor load by adjusting the excitation current of the magnetic powder brake. The data acquisition system consists of NI PXI-1050 chassis, NI PXI-6251 data acquisition card, and FLIR T200 infrared camera. The experimental motor is YE2-132S-4 three-phase asynchronous motor with rated power of 5.5 kW, rated voltage of 380 V, rated current of 11.5 A, speed of 1 440 rpm, rolling bearing model of 6308RZ, rated torque of magnetic powder brake of 100 N·m, and excitation current of 0 A—1 A. The slip power is 8 kW and the output torque can be controlled by the magnetic powder brake controller. The motor current data acquisition with normal bearings installed as well as faulty bearings is collected, and the algorithm is verified.

In the experiments, the non-smooth operating conditions under several different load cases are simulated by setting different values for the magnetic powder brake. The motor current signals of normal bearing and cracked outer ring of the bearing are collected separately, and the magnetic powder brake is adjusted while collecting. So that the motor load shifts between no load, 20%, 30%, 50%, and 80% rated load, and the motor current signal is filtered with a 4 kHz low-pass filter, then the motor current signal with a sampling frequency of 10 kHz and a sampling time of 6 s is collected. And the measured data are analyzed in the Matlab R2018b environment for spectrum analysis. While collecting the current, the FLIR T2200 infrared camera is used to photograph the motor end cover and obtain the infrared image signal.

4.1.2 Data acquisition

1) Current data acquisition

For each data set measured in this experiment, non-smooth operation experiments were collected for the motor operating environment with sampling time periods t_1 to t_2. The operation is shown in Fig.6.

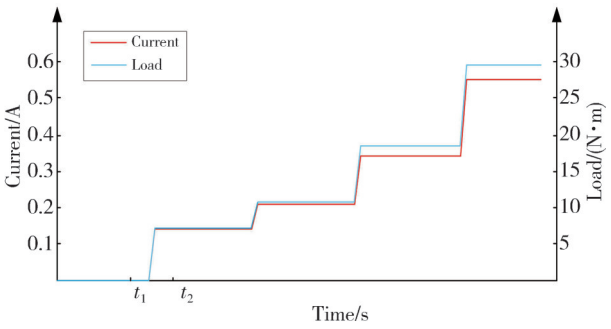

Fig. 6 Excitation current of magnetic powder brake and motor load change curve

Through the current sensor, the current signal under each load change is collected, and the original data with a sampling frequency of 10 kHz and a sampling time (t_2 — t_1) of 6 s is obtained.

The load is changed four times, and one set of data is collected for a single load change, and a total of 16 load change experiments are conducted, i.e., 16 sets of current data are collected for each load change, and a total of 128 sets of data are collected for both bearings. Each group of 6 s raw signal can be split into 24 current training samples by sliding window. And the 128 groups of raw current signals (3 072 current training samples) obtained from the acquisition are decomposed by VMD as shown in Fig.7.

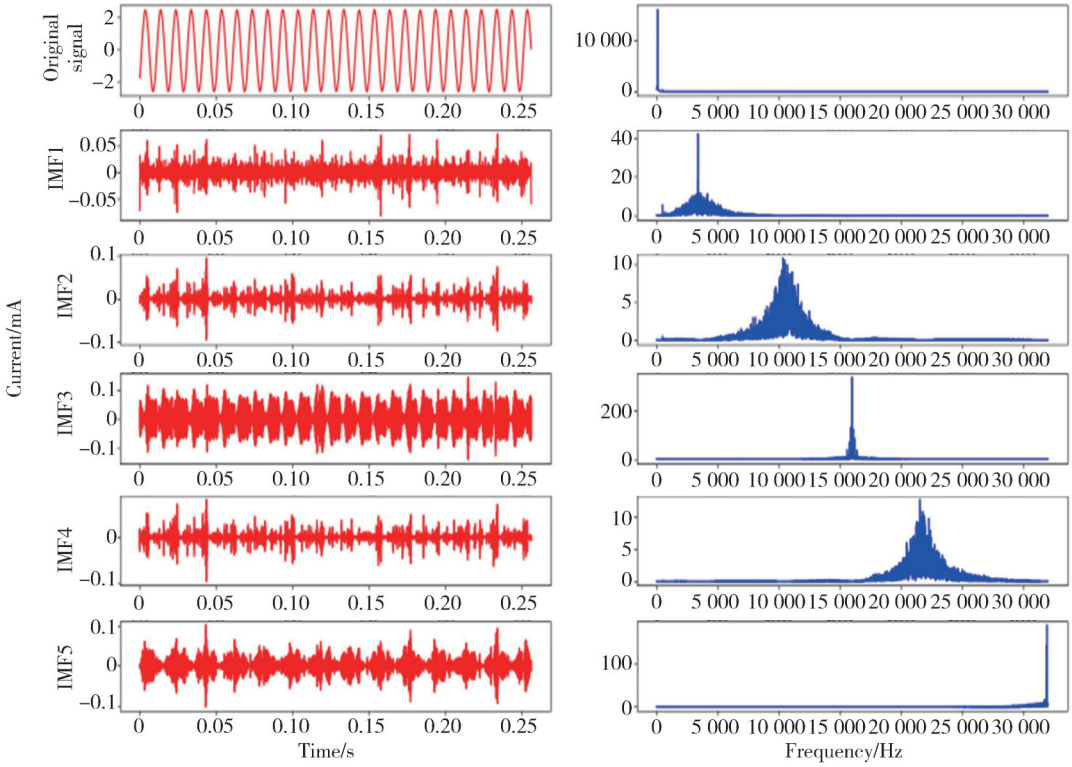

(a) Time domain diagram (b) Frequency domain diagram

Fig. 7 VMD decomposition diagram

The time domain signal of the low frequency band IMF1 is extracted as the signal for subsequent two-dimensionalization. The IMF1 current signal is preprocessed and generated into a neural network available for the two-dimensional grayscale map for training, where 80% of the data set is used as the training set and 20% as the test set for training and testing the neural network, as shown in Table 1.

Table 1 Experimental use of bearing current data

Failure class	Label	Sample size	Total	Training sets	Verification sets
Normal	1	1 536	3 072	2 457	615
Crack	0	1 536			

For the comparison of the subsequent methods, the data collection of bearing fault current data and normal current data will be collected in 16 more groups as the current data of the comparison group.

2) IR image acquisition

Since the motor bearing temperature change is different from the current change, which is gradually and slowly changed, the infrared images were taken in the load state before the load change while the current was acquired. For each set of current signals acquired, one infrared image was captured using a FLIR T200 infrared camera to obtain a total infrared image data set of 128 images, including 64 without faults and 64 with faults. At the same time, an infrared image fault library was established for comparison, and infrared images of bearing outer ring faults were taken at no load, 20%, 30%, 50%, and 80% rated load of the motor, after 10 minutes of stable operation, two images

were taken for each case, and there were 10 infrared images of bearing outer ring faults in the library. Image preprocessing is performed to extract the grayscale feature matrix of the infrared images. After extracting the grayscale feature matrices of the infrared images in the image dataset and the infrared images in the fault library, the cosine similarity of the two grayscale feature matrices is calculated using Eq. (8) to obtain the dataset that is subsequently used to adjust the threshold of the sigmod classifier.

4.2 Experiment results

4.2.1 MCSA troubleshooting

The data set uses a bearing of type 6308, which is a deep groove ball bearing, so the bearing contact angle $\theta=0^{\circ}$, and the bearing outer raceway diameter $D_o=$ 90 mm, inner raceway diameter $D_i=40$ mm. So the knuckle diameter $D_c=65$ mm, rolling body diameter $D_b=15.081$ mm, a total of 8 rolling bodies, motor speed $S=1\ 440\ \mathrm{r\cdot min^{-1}}$. It is possible to calculate the rolling bearing fault vibration characteristic component[9].

The rotational frequency of the motor f_r is

$$f_r=\frac{S}{60}=\frac{1\ 440}{60}=24\ \mathrm{Hz}. \tag{12}$$

The characteristic frequency f_o of bearing outer ring failure vibration is

$$f_o=\frac{n}{2}f_r\left(1-\frac{D_b}{D_c}\cos\theta\right)=\frac{8}{2}\times 24\times\left(1-\frac{15.081}{65}\cos 0^{\circ}\right)=73.73\ \mathrm{Hz}. \tag{13}$$

Motor bearing outer ring sideband fault characteristic frequency is

$$|f_e\pm nf_o|=|50\pm 73.73n|=23.73\&123.73\&197.46\ \mathrm{Hz}, \tag{14}$$

where $n=1,2,3,\cdots$; f_e is the power supply fundamental frequency.

The spectrum is obtained by FFT transformation of the current data, and the spectrum analysis is performed for the current with and without faults, and the spectrum of the power supply frequency ($f_e=50$ Hz) is clearly shown in Fig.8 (a).

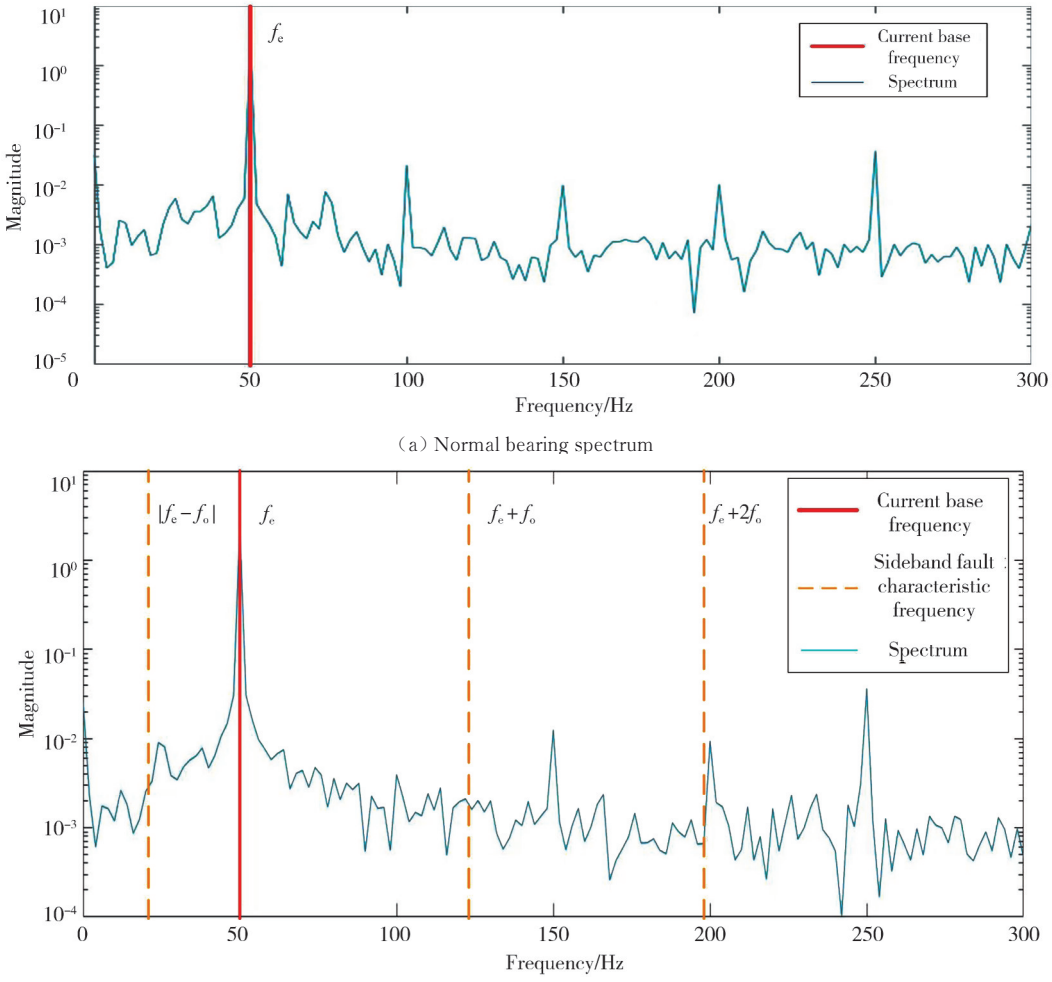

(a) Normal bearing spectrum

(b) Faulty bearing spectrum

Fig. 8 Bearing signal spectrum

However, in the case of a fault, the outer ring fault vibration characteristic component of the current is not clearly shown in the current signal spectrum, as in Fig. 8(b), and the bearing outer ring fault is difficult to extract from the motor current signal for analysis.

4.2.2 Methodology

The proposed motor current and infrared image fusion method for bearing outer ring fault diagnosis firstly trains the neural network using a dataset of 2 457 current training samples, and after the training, the accuracy of the trained CNN is evaluated with 615 current evaluation samples. A total of 130 iterations of this neural network training were performed. The training and testing results of the network are shown in Fig. 9.

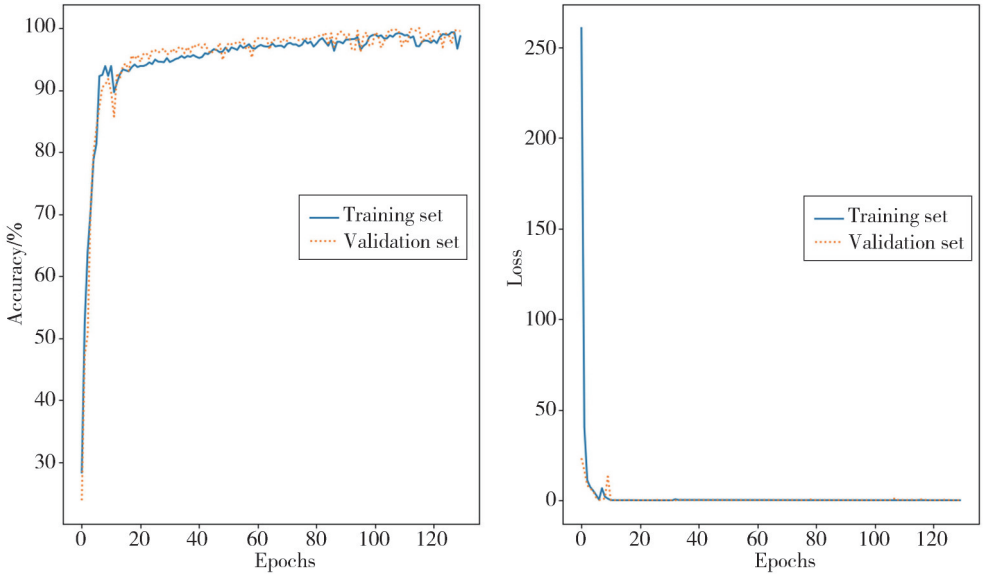

(a) Training and validation of accuracy (b) Training and validation loss

Fig. 9 Neural network training results

At 80 iterations, the training and validation accuracies lie in an interval range. 2 457 current training samples are output by the current classification model completed by training, and the probabilities of each sample being judged as fault-free are $p_1^{1,1}, p_1^{1,2}, \cdots, p_1^{1,2\,457}$ and the probabilities of each sample being judged as fault are $p_1^{2,1}, p_1^{2,2}, \cdots, p_1^{2,2\,457}$. At the same time, the infrared images corresponding to the acquisition current are input into the completed training infrared image classification model. 2 457 infrared image samples, the probabilities of each sample judging the bearing to be fault-free are $p_2^{1,1}, p_2^{1,2}, \cdots, p_2^{1,2\,457}$, and the probabilities of each sample judging the bearing to be faulty are $p_2^{2,1}, p_2^{2,2}, \cdots, p_2^{2,2\,457}$. Therefore, the training set of the fusion algorithm is

$$\boldsymbol{P}_{\text{training}} = \begin{bmatrix} p_1^{1,1} & p_1^{2,1} & p_2^{1,1} & p_2^{2,1} \\ p_1^{1,2} & p_1^{2,2} & p_2^{1,2} & p_2^{2,2} \\ \vdots & \vdots & \vdots & \vdots \\ p_1^{1,2\,457} & p_1^{2,2\,457} & p_2^{1,2\,457} & p_2^{2,2\,457} \end{bmatrix}.$$

Using the training set $\boldsymbol{P}_{\text{training}}$, the weighting factors W_1 and W_2 are trained by the training method to obtain the weighting factors W_1 and W_2 applicable to the fusion algorithm with the objective of minimizing the cross-entropy loss.

The data is passed through t-SNE to visualize the layer output of the model. As seen in Fig. 10(a), the original data points are mixed together and indistinguishable. As seen in Fig. 10(b), the diagnostic accuracy is around 95.76% when the samples of the current comparison group are input to the trained current diagnosis model for fault diagnosis. And the corresponding infrared image comparison group samples are input into the infrared image diagnosis model, and the output is as seen in Fig. 10(c), with a diagnostic accuracy of about 94.3%. Subsequently, using the decision-level fusion algorithm, after training with the corresponding weights of the acquired current signals, the same samples are used for validation, as seen in Fig. 10(d), and the diagnostic accuracy is improved to about 98.85%.

In order to verify that the proposed method has better performance for motor rolling bearing fault diagnosis, the motor current signal diagnosis methods in the Refs. [10] and [20] are trained using the current training dataset, and the same comparison group samples are used for accuracy verification, as shown in Table 2. The fault diagnosis accuracies relying only on motor current data are 90.16% and 96.54%, and the diagnosis effect is not as good as the bearing fault diagnosis effect of the diagnosis model fused with current data and infrared

image data. In order to further verify the effectiveness of the proposed method, the same motor current data set proposed in this paper is used to fuse the current data with infrared images at the decision-making level by using support vector machine (SVM), multi-layer perceptron (MLP), and K-nearest neighbor algorithm (KNN). The diagnostic accuracy rate is shown in Table 2.

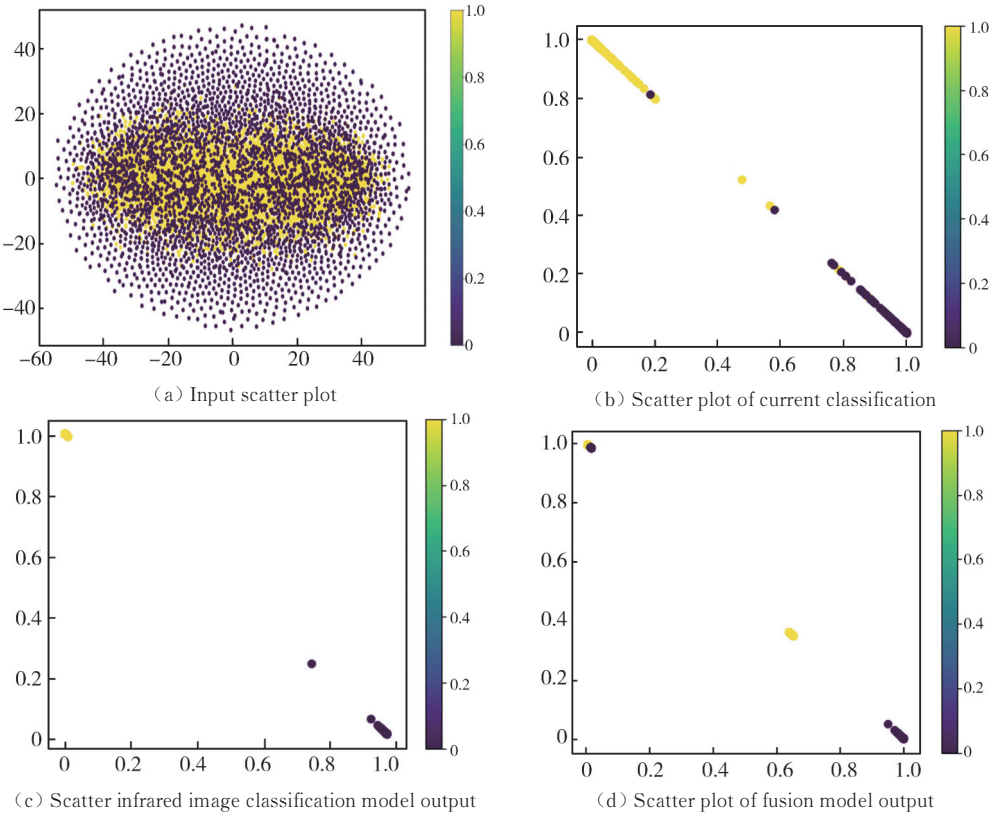

(a) Input scatter plot

(b) Scatter plot of current classification

(c) Scatter infrared image classification model output

(d) Scatter plot of fusion model output

Fig. 10 Scatter plot of model output model output

Table 2 Comparison diagnosis results of fusion algorithms

Algorithm	Configuration	Accuracy/%
CNN	3 convolutional layers, 3 pooling layers, 2 fully connected layers, softmax classification	95.76
FCN[10]	5 nodes, sigmoid activation function	90.16
EMD+PCA+ANN[20]	1 input layer, 1 hidden layer, 1 output layer	96.54
kNN+IR image fusion	k=3	96.82
SVM+IR image fusion	Linear kernel function, sigmoid classification	97.64
MLP+IR image fusion	1 input layer, 2 hidden layers, 1 output layer, softmax classification	97.98
CNN+IR image fusion	This paper fuses algorithms	98.85

The diagnosis accuracy of CNN using current signal alone is low, only about 95.76%, while the fusion of current signal and infrared image signal for diagnosis will significantly improve the accuracy of fault diagnosis. Among several algorithms, the fusion of CNN and infrared image has the best diagnosis effect, and the fault diagnosis accuracy rate can reach 98.85%.

5 Conclusions

Due to the complex and changing working environment of the motor, load changes are often generated, which leads to the amplitude and phase of the characteristic components of the bearing fault changing with time, presenting a time-varying non-smooth characteristic, and it is difficult to carry out accurate diagnosis of the motor bearing fault by time-frequency analysis. The infrared image, as a new type of fault diagnosis signal, can characterize the operation status of the object under test by its temperature. A fault diagnosis method was proposed for rolling bearings of AC motors based on the fusion of current and infrared image information. The method firstly decomposed the current signal using VMD and extracted the low frequency band current signal, then transformed the extracted current signal into a two-dimensional map applicable to CNN and classified it using CNN and softmax classifier. At the same time, it extracted the grayscale feature matrix of the infrared image, calculated the similarity with the existing fault bearing image in the library and classified it using sigmod classifier. Finally, it could be used for fault

diagnosis by decision-level fusion model. When the motor rolling bearing fault was diagnosed, this method could use deep learning to automatically extract effective features from the motor current signal and fuse them with the infrared image to fully exploit the information redundancy and complementarity of the motor current signal and the bearing infrared image to improve the accuracy of motor bearing fault diagnosis. The experimental results showed that the proposed method could effectively and accurately diagnose bearing faults in motors operating under non-smooth operating conditions.

Acknowledgement

This work was supported by National Natural Science Foundation of China (No.61903291); Shaanxi Province Key R&D Program (No.2022GY-134).

Declaration of conflicting interests

The authors have no conflict of interests related to this publication.

References

[1] LEE D, SIU V, CRUZ R. Convolutional neural net and bearing fault analysis//International Conference on Data Mining (DMIN). The Steering Committee of The World Congress in Computer Science, Computer Engineering and Applied Computing (WorldComp), December 12-16, 2016, Barcelona, Spain. New York: IEEE, 2016: 194-200.

[2] TIAN Y L, LIU X Y. A deep adaptive learning method for rolling bearing fault diagnosis using immunity. Tsinghua Science and Technology, 2019, 24(6): 750-762.

[3] YANG P, SU Y C. Falut diagnosis of rolling bearing based on convolution gated recurrent network. Journal of Aerospace Power, 2019, 34(11): 2432-2439.

[4] BIAN H, WANG X L, DENG Z Q. Bearing fault detection for brushless DC motors based on stator current. Journal of Nanjing University of Aeronautics and Astronautics, 2020, 52(2): 224-231.

[5] QI R S, FAN J, LI Y T, et al. A fault diagnosis method of wind turbine bearings based on an enhanced morphological filter. Journal of Vibration and Shock, 2021, 40(4): 212-220.

[6] SCHOEN R R, HABETLER T G, KAMRAN F, et al. Motor bearing damage detection using stator current monitoring. IEEE Transactions on Industry Applications, 1995, 31(6): 1274-1279.

[7] BLODT M, GRANJON P, RAISON B, et al. Models for bearing damage detection in induction motors using stator current monitoring. IEEE Transactions on Industrial Electronics, 2008, 55(4): 1813-1822.

[8] SONG X J, HU J T, ZHU H Y, et al. Effects of the slot harmonics on the stator current in an induction motor with bearing fault. Mathematical Problems in Engineering, 2017, 2017(1): 2640796.

[9] HAN Q K, DING Z, XU X P, et al. Stator current model for detecting rolling bearing faults in induction motors using magnetic equivalent circuits. Mechanical Systems and Signal Processing, 2019, 131: 554-575.

[10] KARATZINIS G, BOUTALIS Y S, KARNAVAS Y L. Motor fault detection and diagnosis using fuzzy cognitive networks with functional weights//2018 26th Mediterranean Conference on Control and Automation (MED), June 19-22, 2018, Zadar, Croatia. New York: IEEE, 2018: 709-714.

[11] BAGAVATHIAPPAN S, SARAVANAN T, GEORGE N P, et al. Condition monitoring of exhaust system blowers using infrared thermography. Insight, 2008, 50(9) 512-515.

[12] SUN B, WANG Y W, YANG L. Study of fault diagnosis of induction motor bearing based on infrared inspection. Electric Machines and Control, 2012, 16(1): 50-55.

[13] AZEEZ A A, ALKHEDHER M, GADALA M S. Thermal imaging fault detection for rolling element bearings//2020 Advances in Science and Engineering Technology International Conferences (ASET). Dubai, United Arab Emirates. New York: IEEE, 2020: 1-5.

[14] HOANG D T, KANG H J. A motor current signal-based bearing fault diagnosis using deep learning and information fusion. IEEE Transactions on Instrumentation and Measurement, 2020, 69(6): 3325-3333.

[15] HOU X G, WU Z G, XIA L, et al. Bearing fault detection method for induction motor based on fusion analysis. Journal of Data Acquisition & Processing, 2006(1): 113-117.

[16] WANG H X, WANG B, DONG X Z, et al. Heterogeneous multi-parameter feature-level fusion for multi-source power sensing terminals: fusion mode, fusion framework and application scenarios. Transactions of China Electrotechnical Society, 2021, 36(7): 1314-1323.

[17] STACK J R, HABETLER T G, HARLEY R G. Fault classification and fault signature production for rolling element bearings in electric machines//4th IEEE International Symposium on Diagnostics for Electric Machines, Power Electronics and Drives, 2003. SDEMPED. Atlanta, GA, USA. New York: IEEE, 2003: 172-176.

[18] DRAGOMIRETSKIY K, ZOSSO D. Variational mode decomposition. IEEE Transactions on Signal Processing, 2014, 62(3): 531-544.

[19] LI J, GUO J Y, LIU Y C, et al. Vietnamese combinational ambiguity disambiguation based on weighted voting method of multiple classifier. Computer Science, 2018, 45(1): 167-172.

[20] JIANG X J, MALIK H, PANDA S K. An optimized intelligent technique for bearing fault diagnosis using motor

current signal analysis//2022 International Power Electronics Conference (IPEC-Himeji 2022-ECCE Asia), May 15-19, 2022, Himeji, Japan. New York: IEEE, 2022: 730-735.

基于电流与红外图像异构数据融合的交流电机滚动轴承故障诊断方法

刘沛津[1], 郭子辰[1], 何 林[2*], 晏东阳[1], 张香瑞[1]

1. 西安建筑科技大学 机电工程学院, 陕西 西安 710055;
2. 西安建筑科技大学 理学院, 陕西 西安 710055

摘 要: 为提高电机在非平稳工况下运行时滚动轴承故障诊断的准确率, 本文提出一种基于电流与红外图像异构数据融合的交流电机滚动轴承故障诊断方法。首先, 使用VMD分解电机电流信号, 提取轴承故障信号所在的低频段分量; 在此基础上, 将低频段电流信号转化为适用于卷积神经网络的二维图, 并利用卷积神经网络及softmax分类器对数据集进行分类。其次, 对红外图像进行图像分割并提取故障特征, 从而与库中故障轴承红外图像进行相似度计算, 进一步利用sigmod分类器对数据进行分类。最后, 引入一种决策级融合的方法, 将电流信号与红外图像信号诊断结果按权重进行融合, 获得电机轴承故障诊断结果。通过实验验证, 本文提出的故障诊断方法在载荷变动情况下均可以进行电机轴承外环故障诊断, 故障诊断的准确率可达98.85%。

关键词: 电流信号; 红外图像; 决策级融合; 滚动轴承; 故障诊断

引用格式: LIU Peijin, GUO Zichen, HE Lin, et al. Fault diagnosis method of AC motor rolling bearing based on heterogeneous data fusion of current and infrared image. Journal of Measurement Science and Instrumentation, 2024, 15(4): 558-570.